Multiparticle Interactions for Ultracold Atoms in Optical Tweezers: Cyclic Ring-Exchange Terms

Annabelle Bohrdt,[1,2,†] Ahmed Omran,[3,†] Eugene Demler,[3] Snir Gazit,[4] and Fabian Grusdt[5,2,1,*]

[1]Department of Physics and Institute for Advanced Study, Technical University of Munich, 85748 Garching, Germany
[2]Munich Center for Quantum Science and Technology (MCQST), Schellingstrasse 4, D-80799 München, Germany
[3]Department of Physics, Harvard University, Cambridge, Massachusetts 02138, USA
[4]Racah Institute of Physics and The Fritz Haber Research Center for Molecular Dynamics, The Hebrew University, Jerusalem 91904, Israel
[5]Department of Physics and Arnold Sommerfeld Center for Theoretical Physics (ASC), Ludwig-Maximilians-Universität München, Theresienstrasse 37, München D-80333, Germany

(Received 15 October 2019; accepted 16 January 2020; published 19 February 2020)

Dominant multiparticle interactions can give rise to exotic physical phases with anyonic excitations and phase transitions without local order parameters. In spin systems with a global SU(N) symmetry, cyclic ring-exchange couplings constitute the first higher-order interaction in this class. In this Letter, we propose a protocol showing how SU(N)-invariant multibody interactions can be implemented in optical tweezer arrays. We utilize the flexibility to rearrange the tweezer configuration on short timescales compared to the typical lifetimes, in combination with strong nonlocal Rydberg interactions. As a specific example, we demonstrate how a chiral cyclic ring-exchange Hamiltonian can be implemented in a two-leg ladder geometry. We study its phase diagram using density-matrix renormalization group simulations and identify phases with dominant vector chirality, a ferromagnet, and an emergent spin-1 Haldane phase. We also discuss how the proposed protocol can be utilized to implement the strongly frustrated J–Q model, a candidate for hosting a deconfined quantum critical point.

DOI: 10.1103/PhysRevLett.124.073601

Introduction.—Ultracold atoms in optical lattices have become a versatile platform for performing analog quantum simulations, with widely tunable interactions [1] and the ability to control the single-particle band structure [2–8]. Using atoms with permanent electric or magnetic dipole moments [9] or in Rydberg states [10] allows us to study systems with long-range dipole-dipole or van der Waals interactions, which can mimic the long-range Coulomb repulsion between electrons in a solid. These ingredients can be combined to study exotic phenomena in strongly correlated many-body systems, related, for example, to quantum magnetism [11–17] or the fractional quantum Hall effect [18–20]. Leveraging the capabilities of ultracold atoms, such experiments promise new insights, for example, to directly measure topological invariants [21–25] or image the quantum mechanical wave function with single-site resolution [26–31].

In this Letter, we go beyond the two-body interactions realized so far and propose a general protocol to implement highly symmetric multiparticle interactions with ultracold atoms in optical tweezer arrays. Multiparticle interactions can lead to exotic ground states with intrinsic topological order [32,33], with applications for quantum computation [34,35], and they are an important ingredient for realizing lattice gauge theories [36–39] central to the quantum simulation of high-energy phenomena or deconfined quantum criticality [40,41]. If these higher-order couplings possess additional symmetries, e.g., SU(N) invariance in spin systems, models with strong frustration can be realized for which the ground states are strongly correlated quantum liquids.

In condensed matter systems, multispin interactions of this type emerge from higher-order virtual processes [42], leading to corrections to the pairwise Heisenberg couplings of SU(2) spins in a half filled Hubbard model. These cyclic ring-exchange terms play a role in frustrated quantum magnets like solid ^{3}He [43] and possibly also for the phase diagram of high-T_c cuprate superconductors [44,45]. In this Letter, we demonstrate how such multispin interactions can be realized and independently tuned in ultracold atom systems without resorting to high-order virtual processes.

A promising route to implementing multiparticle processes is to use strong interactions between atoms in different Rydberg states representing spin degrees of freedom (d.o.f.). This allows us to build a versatile quantum simulator that can be used to realize ring-exchange interactions in spin systems by representing them as sums of products of Pauli matrices [46] or to implement local constraints giving rise to emergent dynamical gauge fields [47,48].

Here we follow a similar strategy, but propose to combine strong Rydberg interactions with the capabilities to quickly change the spatial configuration of atoms

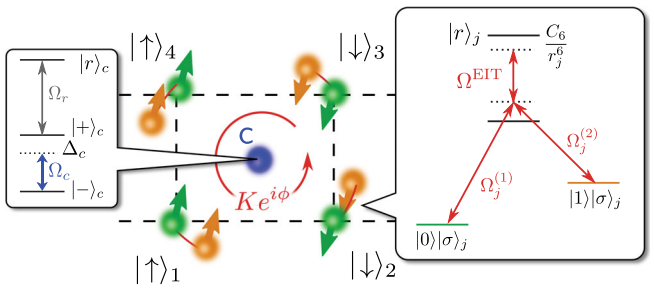

FIG. 1. Proposed setup: SU(2)-invariant chiral cyclic ring-exchange interactions can be realized by combining state-dependent lattices generated by optical tweezer arrays and strong Rydberg interactions with a central Rydberg-dressed control qubit (C). The auxiliary states $|\tau = 1\rangle|\sigma\rangle$ with $\sigma = \uparrow, \downarrow$ (orange) of the atoms on the sites of the plaquette are subject to a state-dependent tweezer potential, which allows us to permute them coherently around the center. Our protocol makes use of stroboscopic π pulses between the physical states $\tau = 0$ (green) and the auxiliary states $\tau = 1$, which only take place collectively on all sites and are conditioned on the absence of a Rydberg excitation in the control atom.

trapped in optical tweezer arrays [49–53]. We consider general lattice models with one N-component particle per lattice site (fermionic or bosonic) and show, as an explicit example, how a general class of SU(N)-invariant chiral cyclic ring-exchange (CCR) interactions can be realized. They are described by a Hamiltonian ($\hbar = 1$)

$$\hat{\mathcal{H}}_{\mathrm{CCR}}(\phi) = K\sum_p (e^{i\phi}\hat{P}_p + e^{-i\phi}\hat{P}_p^\dagger), \tag{1}$$

where the sum is over all plaquettes p of the underlying lattice, the operator $\hat{P}_p^\dagger$ ($\hat{P}_p$) cyclically permutes the spin configuration on plaquette p in the clockwise (counterclockwise) direction, and ϕ is a tunable complex phase. A generalization to finite hole doping, with zero or one particle per lattice site, is straightforward.

Nonchiral cyclic ring-exchange interactions, realized by Eq. (1) for $\phi = 0$, are believed to play a role in the high-T_c cuprate compounds. These materials can be described by the 2D Fermi-Hubbard model on a square lattice, with weak couplings between multiple layers in the z direction [54]. For the relevant on site interactions U, which dominate over the nearest-neighbor tunneling $t \ll U$, this model can be simplified by an expansion in powers of t/U. To lowest order, one obtains a t–J model [55] with nearest-neighbor spin-exchange interactions of strength $J = 4t^2/U$. Next to leading order, cyclic ring-exchange terms on the plaquettes of the square lattice contribute with strength $K = 20t^4/U^3$. By comparison of first principle calculations and measurements in the high-temperature regime, it was shown that $K \approx 0.13 \times J$ in La_2CuO_4 [56], but its effect on the phase diagram remains debated. In ultracold atoms, similar higher-order processes have been used to realize nonchiral cyclic ring-exchange couplings [57,58].

We start by explaining the general scheme using the example of CCR interactions. Our method is more versatile, however, and we discuss how it can be adapted to implement the J–Q model, which has been proposed as a candidate system realizing deconfined quantum criticality [40,41]. We also analyze the phase diagram of the CCR Hamiltonian (1) in a ladder geometry, with exactly one SU(2) spin per lattice site. We show that the phase diagram contains a gapped Haldane phase with topologically protected edge states [59–61] at intermediate values of $\pi/4 \lesssim \phi \lesssim 3\pi/4$, a ferromagnetic phase for $\phi \gtrsim 3\pi/4$, and a dominant vector chirality for $\phi \lesssim \pi/4$.

Implementation.—For simplicity, we consider a single plaquette, restrict ourselves to $N_p = 4$ sites and assume SU(2) symmetry, see Fig. 1. Generalizations of our scheme to more than one plaquette, $N_p \neq 4$, and SU(N) symmetry are possible (see Supplemental Material [62]).

Each of the four sites, labeled $j = 1, \ldots, 4$, consists of a static optical tweezer trapping a single atom, where recently demonstrated rearrangement methods [49–53] allow for populating each site with high fidelity. We assume that the atoms remain in the vibrational ground states of the microtraps throughout the sequence. Every atom has two internal states $\sigma = \uparrow, \downarrow$, which we use to implement an effective spin-1/2 system. As a specific configuration we suggest to use ^{133}Cs atoms and utilize their $F = 3$, $m_F = 2, 3$ hyperfine states to represent the two spins. Optical pumping with site-resolved addressing can then be employed to prepare arbitrary initial spin patterns [58] and study their dynamics under Eq. (1).

The key ingredient for our proposed implementation of CCR interactions is to realize collective permutations of the entire spin configuration in the plaquette. This can be achieved by physically rotating the tweezer array around the center of the plaquette, while ensuring that the motional and spin states of the atoms are preserved and coherence is not lost. The effect of clockwise rotations of the microtraps on the spin states is described by the operator $\hat{P}$,

$$\hat{P}|\sigma_1, \sigma_2, \sigma_3, \sigma_4\rangle = |\sigma_4, \sigma_1, \sigma_2, \sigma_3\rangle. \tag{2}$$

Optimized trajectories can be chosen to cancel heating effects from the motion [65]. These require a timescale set by the quantum speed limit that scales as the inverse energy gap of each trap $t_{\mathrm{rot}} \sim 1/\Delta\varepsilon$. For deep trapping potentials where $\Delta\varepsilon \approx 150$ kHz, rotation times of $t_{\mathrm{rot}} < 10\ \mu$s are achievable.

In contrast to Eq. (2), the effective Hamiltonian leads to a superposition of permuted and nonpermuted states in every infinitesimal time step Δt, as can be seen from a Taylor expansion: $e^{-i\hat{\mathcal{H}}_{\mathrm{CCR}}\Delta t} = 1 - i\hat{\mathcal{H}}_{\mathrm{CCR}}\Delta t$. To create such superposition states in our time evolution, we assume

that every atom has a second internal d.o.f. labeled by $\tau = 0, 1$. Concretely, we propose to realize the new states $|\tau = 1\rangle|\sigma\rangle$ in ^{133}Cs atoms by $F = 4$, $m_F = 3$, 4 hyperfine levels, where $m_F = 3$ ($m_F = 4$) corresponds to $\sigma = \downarrow$ ($\sigma = \uparrow$). These additional levels will be used as auxiliary states, whereas the states $|\tau = 0\rangle|\sigma\rangle$ introduced before—implemented as $F = 3$, $m_F = 2$, 3 levels in ^{133}Cs—realize the physical spin states.

One part of our protocol consists of a permutation of the spins σ, but only in the manifold of auxiliary states. This step requires a total time $t_{\rm rot}$ and can be described by the unitary transformations

$$\hat{U}_+ = \prod_j |1\rangle_j\langle 1| \otimes \hat{P} + \prod_j |0\rangle_j\langle 0| \otimes \hat{\mathbf{1}}_\sigma, \qquad \hat{U}_- = \hat{U}_+^\dagger. \tag{3}$$

To implement this evolution, two sets of optical tweezer arrays can be used, of which only one is rotating. We suggest to realize it by the near-magic wavelength $\lambda_{\rm magic} \approx 871.6$ nm in ^{133}Cs, which strongly confines atoms in the state $\tau = 1$, but almost does not affect atoms in $\tau = 0$. By applying $\hat{U}_\pm$ to superposition states with either all atoms in $\tau = 1$ or all atoms in $\tau = 0$, one can realize the desired superpositions of permuted and nonpermuted spin configurations. Such states can be realized by collective π pulses conditioned upon a control qubit trapped in the center of the plaquette [66], as described next.

If the control atom is in the state $|+\rangle_c$, it is transferred to a Rydberg state $|r\rangle_c$ with a resonant π pulse and Rabi frequency Ω_r, see Fig. 1. If the control atom is in state $|-\rangle_c$, the laser Ω_r is off-resonant and no Rydberg excitation is created. Next, a Raman transition by lasers $\Omega_j^{(1)}$, $\Omega_j^{(2)}$ through an intermediate Rydberg state $|r\rangle_j$ is used to implement a π pulse transferring the physical states $|0\rangle_j$ to $|1\rangle_j$, without changing their spin state $|\sigma\rangle_j$. In the presence of a coupling field $\Omega^{\rm EIT}$ that establishes two-photon resonance to the Rydberg state with each Raman laser, electromagnetically induced transparency (EIT) [67] suppresses the transition $|0\rangle_j \leftrightarrow |1\rangle_j$. However, the EIT condition is lifted by the Rydberg blockade mechanism if the control atom is in the Rydberg state $|r\rangle_c$ [66], enabling the transfer. After the transfer is complete, another π pulse by Ω_r is applied to the control atom. This ensures that the control atom remains trapped during the protocol, even if the Rydberg excited state is not subject to a trapping potential. In summary, this part is described by the unitary transformation

$$\hat{U}_{\rm sw} = |+\rangle_c\langle +| \otimes \left(\prod_j |1\rangle_j\langle 0| + \text{H.c.}\right) \otimes \hat{\mathbf{1}}_\sigma + |-\rangle_c\langle -| \otimes \hat{\mathbf{1}}_\tau \otimes \hat{\mathbf{1}}_\sigma. \tag{4}$$

The total time required to implement this switch (sw) is denoted by $t_{\rm sw}$.

Finally, we need to introduce quantum dynamics between the states of the control atom. This can be realized by a dressing laser Ω_c driving transitions between $|\pm\rangle_c$, at a detuning Δ_c. These dynamics take place over a period of time t_c and are described by the unitary evolution $\hat{U}_c = e^{-i\hat{\mathcal{H}}_c t_c}$ with $\hat{\mathcal{H}}_c = \Delta_c|+\rangle_c\langle +| + \Omega_c(|+\rangle_c\langle -| + \text{H.c.})$. During the remaining steps of the protocol, Eqs. (3) and (4), we assume that $\Omega_c = 0$ is off and the control atom picks up a phase $\pm\varphi_c$ if it is in state $|+\rangle_c$. This phase can be adjusted by the detuning Δ_c and the duration $t_{\rm rx} = 2t_{\rm sw} + t_{\rm rot}$, during which the time evolution of the control is $\hat{U}_{\pm\varphi_c} = |+\rangle_c\langle +|e^{\mp i\varphi_c} + |-\rangle_c\langle -|$.

The complete protocol is summarized in Fig. 2. It consists of a periodic repetition of the individual steps described above. At the discrete time steps nT, where $T = 2(t_c + t_{\rm rx})$, the unitary evolution is described by an effective Hamiltonian $\hat{\mathcal{H}}_{\rm eff}$,

$$e^{-inT\hat{\mathcal{H}}_{\rm eff}} = (\hat{U}_T)^n = (\hat{U}_{{\rm rx},+}\hat{U}_c\hat{U}_{{\rm rx},-}\hat{U}_c)^n, \tag{5}$$

where we defined $\hat{U}_{{\rm rx},\pm} = \hat{U}_{\rm sw}(\hat{U}_{\pm\varphi_c} \otimes \hat{U}_\pm)\hat{U}_{\rm sw}$. As will be shown below, $\hat{\mathcal{H}}_{\rm eff}$ realizes CCR interactions with a tunable phase $\phi = -\varphi_c$ and amplitude

$$K = -\frac{1}{2T}(t_c\Delta_c)\left(\frac{\Omega_c}{\Delta_c}\right)^2, \tag{6}$$

provided that

$$t_c \ll 2\pi/\Delta_c, \qquad \Omega_c \ll \Delta_c. \tag{7}$$

Now we estimate the strength $|K|$ of the CCR interactions that can be achieved with the proposed setup. To satisfy Eq. (7), we assume $\Omega_c = 0.2\Delta_c$ and $t_c\Delta_c = 0.4$. For

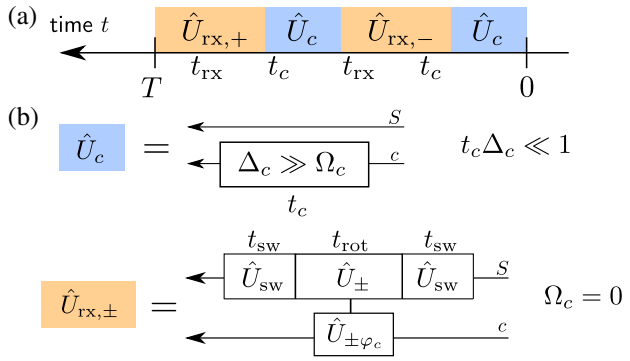

FIG. 2. Proposed protocol: The sequence in (a) is repeated periodically with period $T = 2(t_c + t_{\rm rx})$. When $t_c \ll 2\pi/\Delta_c$, $1/\Omega_c$ it implements a Trotterized time evolution of the effective Hamiltonian (8), which realizes CCR couplings when $\Delta_c \gg \Omega_c$. The individual time steps are illustrated in (b).

a rotation time $t_{\rm rot} = 10\ \mu$s and assuming $t_{\rm sw}, t_c \ll t_{\rm rot}$, a reasonable strength of $K/\hbar = 50\ {\rm Hz} \times 2\pi$ can be achieved. This requires $\Omega_c/2\pi \gg 1.3$ kHz, which can be easily realized; the condition $t_{\rm sw} \ll 10\ \mu$s can also be met, as the Rydberg π pulses on the control atom can be executed in $\sim$100 ns each, and the Raman transfer between the states $|0\rangle_j$ and $|1\rangle_j$ can be driven with coupling strengths above 1 MHz.

Effective Hamiltonian.—Next we show that our protocol realizes the Hamiltonian in Eq. (1). When $t_c/2\pi \ll 1/\Delta_c, 1/\Omega_c$, we can write $\hat{U}_c = 1 - i\hat{\mathcal{H}}_c t_c$ and calculate $\exp[-i\hat{\mathcal{H}}_{\rm eff}T]$ to leading order in t_c. Equations (3) and (4) yield

$$\hat{\mathcal{H}}_{\rm eff} = \frac{t_c}{T}\{2\Delta_c|+\rangle_c\langle+| + \Omega_c[|-\rangle_c\langle+|(1+e^{i\varphi_c}\hat{P}^\dagger) + {\rm H.c.}]\}. \quad (8)$$

When $\Omega_c \ll \Delta_c$ we can eliminate the state $|+\rangle_c$, which is only virtually excited. This further simplifies the effective Hamiltonian and we obtain

$$\hat{\mathcal{H}}_{\rm eff} = K(2 + e^{-i\varphi_c}\hat{P} + e^{i\varphi_c}\hat{P}^\dagger). \quad (9)$$

Up to the energy shift $2K$ this realizes CCR interactions in an isolated plaquette. The result can be extended to multiple plaquettes by implementing the Trotterized time step $\hat{U}_T$ interchangeably on inequivalent plaquettes.

Two-leg ladder with CCR.—Now we discuss the physics of the SU(2) CCR Hamiltonian in a two-leg ladder. We vary the phase ϕ in the Hamiltonian (1) with $K = 1$ and calculate the ground state phase diagram using the density-matrix renormalization group (DMRG). For $\phi = \pi$, the ground state has ferromagnetic correlations, see Fig. 3(c). It can be readily seen that the variational energy $\langle\hat{\mathcal{H}}_{\rm CCR}(\pi)\rangle$ is minimized for ferromagnetic configurations. In the sector $S^z_{\rm tot} = 0$ used in our DMRG in Fig. 3(c), we find phase separation with two ferromagnetic domains of opposite magnetization.

At intermediate ϕ, we find an emergent Haldane phase, with two-fold degenerate states in the entanglement spectrum, see Fig. 3(a). For a finite $S^z_{\rm tot} = 1$, the expectation value $\langle\hat{S}^z_{L,1}\rangle$ at the edge is nonzero, see Fig. 3(b). The spin gap $\Delta E_S = E_{0,S=1} - E_{0,S=0}$, defined as the difference between the ground state energy with and without finite total magnetization, is zero in this phase, since the additional spin can be placed in the spin-1/2 topological edge states of the system without increasing the total energy. We corroborate this picture further by considering the K–K' model with alternating strengths K, K' of the CCR interactions on adjacent plaquettes. In the Supplemental Material [62], we provide an explicitly derivation of a spin-1 model with a gapped Haldane ground state [60,68] for $\phi = \pi/2$ and $K' \ll K$.

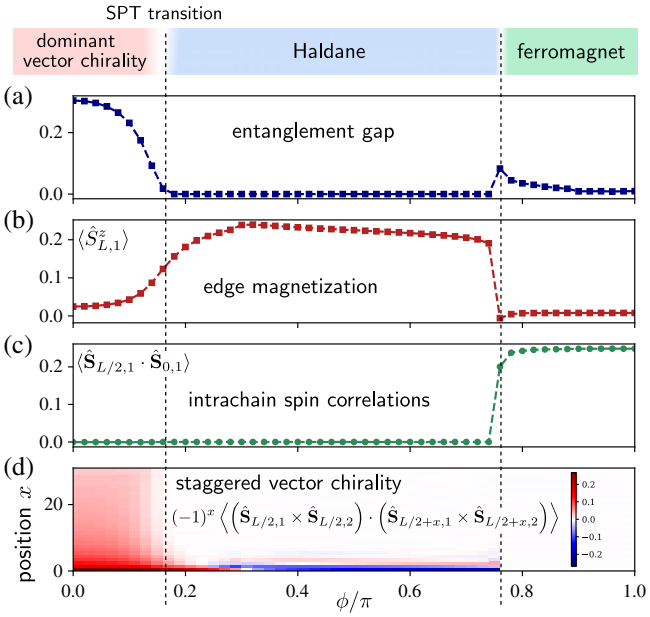

FIG. 3. Phase diagram of the CCR Hamiltonian on a ladder, obtained from DMRG in a system with 64 sites: different observables are evaluated in the ground state of the Hamiltonian (1) to characterize the phases. Upon varying ϕ, three different phases can be identified: (a) a topological Haldane phase featuring a vanishing gap in the entanglement spectrum, (b) edge states with a nonzero local magnetization for $S^z_{\rm tot} = 1$, (c) a symmetry-broken phase around $\phi = \pi$ with long-range ferromagnetic correlations, and (d) a symmetric phase for small ϕ, where the staggered vector chirality remains nonvanishing over long distances.

For small values of ϕ, the ground state of the CCR Hamiltonian is a dominant vector chirality phase, as discussed in Ref. [69]. This phase is characterized by correlations of the form $\hat{\mathbf{S}}_{x,y} \times \hat{\mathbf{S}}_{x',y'}$ in a staggered arrangement around each plaquette. We find that the staggered correlation between different rungs, measured from the center $L/2$ of the chain,

$$(-1)^x\langle(\hat{\mathbf{S}}_{L/2,1} \times \hat{\mathbf{S}}_{L/2,2}) \cdot (\hat{\mathbf{S}}_{L/2+x,1} \times \hat{\mathbf{S}}_{L/2+x,2})\rangle, \quad (10)$$

decays slowly as a function of the distance x and retains significant nonzero values over the considered system sizes, see Fig. 3(d). The transition between the dominant vector chirality and Haldane phases is a symmetry-protected topological (SPT) phase transition.

Using the global SU(2) symmetry, the staggered vector chirality becomes $6\langle\hat{S}^x_{L/2,1}\hat{S}^y_{L/2,2}(\hat{S}^x_{L/2+x,1}\hat{S}^y_{L/2+x,2} - \hat{S}^y_{L/2+x,1}\hat{S}^x_{L/2+x,2})\rangle(-1)^x$. Measuring it requires access to two four-point functions of the form $\langle\hat{S}^\mu_i\hat{S}^\nu_j\hat{S}^\lambda_k\hat{S}^\rho_l\rangle$, which can be detected by making use of local addressing techniques (see, e.g., [70]). To detect the Haldane phase experimentally, we propose to study weakly magnetized systems and image the topological edge states. Alternatively, one could

work in the plaquette basis (see Supplemental Material [62]) and measure the Haldane string order parameter. An interesting future extension would be to use machine learning techniques to retrieve nonlocal order parameters from a series of quantum projective measurements.

Summary and outlook.—In summary, we propose a general method for implementing multibody interactions in ultracold atom experiments using optical tweezer arrays. The approach is particularly useful in the presence of additional, e.g., global SU(N) spin, symmetries. Specifically, we consider a four-body cyclic ring-exchange term, which can be realized with a combination of multiqubit gates based on Rydberg states and movable optical tweezers. We numerically study the ground state of the cyclic ring-exchange Hamiltonian and find different dominant correlation functions as the complex phase of the ring-exchange term is varied.

Our Letter paves the way for future studies of the interplay between ring- and pair-exchange terms, as discussed in Ref. [71] for the nonchiral case $\phi = 0$. In the experimental realization proposed here, it is conceptually straightforward to introduce mobile holes into the system, leading to a finite doping. The interplay between spin and charge d.o.f. could be further studied by adding direct tunneling terms, which lead to rich Hamiltonians in the spirit of t–J-like models. The physics of this type of model is completely unknown and provides an exciting prospect for future theoretical and experimental research. The proposed protocol is versatile enough to implement larger classes of models with multispin interactions, such as the J–Q model [41] (as we discuss in the Supplemental Material [62]). In two dimensions, this model features a phase transition between an antiferromagnet and a valence-bond solid, which has been proposed as a candidate for a deconfined quantum critical point [41]. Moreover, the experimental protocol can be varied to study different types of problems, such as discrete time evolutions of complex models or impurity models, which can be realized by an inclusion of the control qubits into the models.

The authors would like to thank T. Calarco, M. Endres, M. Greiner, A. Kaufman, M. Knap, and M. Lukin for fruitful discussions. A. B. and F. G. acknowledge support from the Technical University of Munich—Institute for Advanced Study, funded by the German Excellence Initiative and the European Union FP7 under Grant No. 291763, the Deutsche Forschungsgemeinschaft (DFG, German Research Foundation) under Germany's Excellence Strategy–EXC-2111–390814868, DFG Grant No. KN1254/1-1, DFG TRR80 (Project F8). A. B. acknowledges support by the Studienstiftung des deutschen Volkes. A. O. acknowledges support from a German Research Foundation (DFG) research fellowship. E. D. acknowledges support by Harvard-MIT CUA, AFOSR-MURI Quantum Phases of Matter (Grant No. FA9550-14-1-0035), AFOSR-MURI: Photonic Quantum Matter (Grant No. FA95501610323), DARPA DRINQS program (Grant No. D18AC00014). S. G. acknowledges support from the Israel Science Foundation, Grant No. 1686/18. F. G. acknowledges support by the Gordon and Betty Moore Foundation through the EPiQS program.

*Corresponding author.
fabian.grusdt@lmu.de
†These authors contributed equally.

[1] I. Bloch, J. Dalibard, and W. Zwerger, Many-body physics with ultracold gases, Rev. Mod. Phys. **80**, 885 (2008).
[2] L. Tarruell, D. Greif, T. Uehlinger, G. Jotzu, and T. Esslinger, Creating, moving and merging dirac points with a fermi gas in a tunable honeycomb lattice, Nature (London) **483**, 302 (2012).
[3] Y.-J. Lin, K. Jimenez-Garcia, and I. B. Spielman, Spin-orbit-coupled Bose-Einstein condensates, Nature (London) **471**, 83 (2011).
[4] M. Aidelsburger, M. Atala, S. Nascimbene, S. Trotzky, Y.-A. Chen, and I. Bloch, Experimental Realization of Strong Effective Magnetic Fields in an Optical Lattice, Phys. Rev. Lett. **107**, 255301 (2011).
[5] L. W. Cheuk, A. T. Sommer, Z. Hadzibabic, T. Yefsah, W. S. Bakr, and M. W. Zwierlein, Spin-Injection Spectroscopy of a Spin-Orbit Coupled Fermi Gas, Phys. Rev. Lett. **109**, 095302 (2012).
[6] J. Struck, C. Ölschläger, M. Weinberg, P. Hauke, J. Simonet, A. Eckardt, M. Lewenstein, K. Sengstock, and P. Windpassinger, Tunable Gauge Potential for Neutral and Spinless Particles in Driven Optical Lattices, Phys. Rev. Lett. **108**, 225304 (2012).
[7] J. Li, W. Huang, B. Shteynas, S. Burchesky, F. C. Top, E. Su, J. Lee, A. O. Jamison, and W. Ketterle, Spin-Orbit Coupling and Spin Textures in Optical Superlattices, Phys. Rev. Lett. **117**, 185301 (2016).
[8] Z. Wu, L. Zhang, W. Sun, X.-T. Xu, B.-Z. Wang, S.-C. Ji, Y. Deng, S. Chen, X.-J. Liu, and J.-W. Pan, Realization of two-dimensional spin-orbit coupling for Bose-Einstein condensates, Science **354**, 83 (2016).
[9] T. Lahaye, C. Menotti, L. Santos, M. Lewenstein, and T. Pfau, The physics of dipolar bosonic quantum gases, Rep. Prog. Phys. **72**, 126401 (2009).
[10] M. Saffman, T. G. Walker, and K. Molmer, Quantum information with Rydberg atoms, Rev. Mod. Phys. **82**, 2313 (2010).
[11] J. Simon, W. S. Bakr, R. Ma, M. E. Tai, P. M. Preiss, and M. Greiner, Quantum simulation of antiferromagnetic spin chains in an optical lattice, Nature (London) **472**, 307 (2011).
[12] D. Greif, T. Uehlinger, G. Jotzu, L. Tarruell, and T. Esslinger, Short-range quantum magnetism of ultracold fermions in an optical lattice, Science **340**, 1307 (2013).
[13] S. Hild, T. Fukuhara, P. Schauß, J. Zeiher, M. Knap, E. Demler, I. Bloch, and C. Gross, Far-From-Equilibrium Spin Transport in Heisenberg Quantum Magnets, Phys. Rev. Lett. **113**, 147205 (2014).
[14] R. A. Hart, P. M. Duarte, T.-L. Yang, X. Liu, T. Paiva, E. Khatami, R. T. Scalettar, N. Trivedi, D. A. Huse, and

R. G. Hulet, Observation of antiferromagnetic correlations in the Hubbard model with ultracold atoms, Nature (London) **519**, 211 (2015).
[15] T. A. Hilker, G. Salomon, F. Grusdt, A. Omran, M. Boll, E. Demler, I. Bloch, and C. Gross, Revealing hidden antiferromagnetic correlations in doped Hubbard chains via string correlators, Science **357**, 484 (2017).
[16] A. Mazurenko, C. S. Chiu, G. Ji, M. F. Parsons, M. Kanasz-Nagy, R. Schmidt, F. Grusdt, E. Demler, D. Greif, and M. Greiner, A cold-atom Fermi-Hubbard antiferromagnet, Nature (London) **545**, 462 (2017).
[17] P. T. Brown, D. Mitra, E. Guardado-Sanchez, P. Schauß, S. S. Kondov, E. Khatami, T. Paiva, N. Trivedi, D. A. Huse, and W. S. Bakr, Spin-imbalance in a 2d Fermi-Hubbard system, Science **357**, 1385 (2017).
[18] N. Gemelke, E. Sarajlic, and S. Chu, Rotating few-body atomic systems in the fractional quantum Hall regime, arXiv:1007.2677v1.
[19] M. E. Tai, A. Lukin, M. Rispoli, R. Schittko, T. Menke, D. Borgnia, P. M. Preiss, F. Grusdt, A. M. Kaufman, and M. Greiner, Microscopy of the interacting Harper-Hofstadter model in the two-body limit, Nature (London) **546**, 519 (2017).
[20] L. W. Clark, N. Schine, C. Baum, N. Jia, and J. Simon, Observation of Laughlin states made of light, arXiv:1907.05872.
[21] M. Atala, M. Aidelsburger, J. T. Barreiro, D. Abanin, T. Kitagawa, E. Demler, and I. Bloch, Direct measurement of the Zak phase in topological Bloch bands, Nat. Phys. **9**, 795 (2013).
[22] F. Grusdt, N. Y. Yao, D. Abanin, M. Fleischhauer, and E. Demler, Interferometric measurements of many-body topological invariants using mobile impurities, Nat. Commun. **7**, 11994 (2016).
[23] N. Fläschner, B. S. Rem, M. Tarnowski, D. Vogel, D.-S. Lühmann, K. Sengstock, and C. Weitenberg, Experimental reconstruction of the Berry curvature in a Floquet Bloch band, Science **352**, 1091 (2016).
[24] T. Li, L. Duca, M. Reitter, F. Grusdt, E. Demler, M. Endres, M. Schleier-Smith, I. Bloch, and U. Schneider, Bloch state tomography using Wilson lines, Science **352**, 1094 (2016).
[25] L. Asteria, D. T. Tran, T. Ozawa, M. Tarnowski, B. S. Rem, N. Fläschner, K. Sengstock, N. Goldman, and C. Weitenberg, Measuring quantized circular dichroism in ultracold topological matter, Nat. Phys. **15**, 449 (2019).
[26] T. Gericke, P. Wuertz, D. Reitz, T. Langen, and H. Ott, High-resolution scanning electron microscopy of an ultracold quantum gas, Nat. Phys. **4**, 949 (2008).
[27] W. S. Bakr, J. I. Gillen, A. Peng, S. Foelling, and M. Greiner, A quantum gas microscope for detecting single atoms in a Hubbard-regime optical lattice, Nature (London) **462**, 74 (2009).
[28] J. F. Sherson, C. Weitenberg, M. Endres, M. Cheneau, I. Bloch, and S. Kuhr, Single-atom-resolved fluorescence imaging of an atomic Mott insulator, Nature (London) **467**, 68 (2010).
[29] M. F. Parsons, A. Mazurenko, C. S. Chiu, G. Ji, D. Greif, and M. Greiner, Site-resolved measurement of the spin-correlation function in the Fermi-Hubbard model, Science **353**, 1253 (2016).
[30] M. Boll, T. A. Hilker, G. Salomon, A. Omran, J. Nespolo, L. Pollet, I. Bloch, and C. Gross, Spin- and density-resolved microscopy of antiferromagnetic correlations in Fermi-Hubbard chains, Science **353**, 1257 (2016).
[31] L. W. Cheuk, M. A. Nichols, K. R. Lawrence, M. Okan, H. Zhang, E. Khatami, N. Trivedi, T. Paiva, M. Rigol, and M. W. Zwierlein, Observation of spatial charge and spin correlations in the 2d Fermi-Hubbard model, Science **353**, 1260 (2016).
[32] N. Read and E. Rezayi, Beyond paired quantum Hall states: Parafermions and incompressible states in the first excited landau level, Phys. Rev. B **59**, 8084 (1999).
[33] A. Kitaev, Anyons in an exactly solved model and beyond, Ann. Phys. (Amsterdam) **321**, 2 (2006).
[34] A. Y. Kitaev, Fault-tolerant quantum computation by anyons, Ann. Phys. (Amsterdam) **303**, 2 (2003).
[35] C. Nayak, S. H. Simon, A. Stern, M. Freedman, and S. D. Sarma, Non-Abelian anyons and topological quantum computation, Rev. Mod. Phys. **80**, 1083 (2008).
[36] H. P. Büchler, M. Hermele, S. D. Huber, M. P. A. Fisher, and P. Zoller, Atomic Quantum Simulator for Lattice Gauge Theories and Ring Exchange Models, Phys. Rev. Lett. **95**, 040402 (2005).
[37] L. Tagliacozzo, A. Celi, A. Zamora, and M. Lewenstein, Optical Abelian lattice gauge theories, Ann. Phys. (Amsterdam) **330**, 160 (2013).
[38] U.-J. Wiese, Ultracold quantum gases and lattice systems: Quantum simulation of lattice gauge theories, Ann. Phys. (Berlin) **525**, 777 (2013).
[39] E. Zohar, J. I. Cirac, and B. Reznik, Quantum simulations of lattice gauge theories using ultracold atoms in optical lattices, Rep. Prog. Phys. **79**, 014401 (2016).
[40] T. Senthil, A. Vishwanath, L. Balents, S. Sachdev, and M. P. A. Fisher, Deconfined quantum critical points, Science **303**, 1490 (2004).
[41] A. W. Sandvik, Evidence for Deconfined Quantum Criticality in a Two-Dimensional Heisenberg Model with Four-Spin Interactions, Phys. Rev. Lett. **98**, 227202 (2007).
[42] P. A. M. Dirac, Quantum mechanics of many-electron systems, Proc. R. Soc. A **123**, 714 (1929).
[43] M. Roger, J. H. Hetherington, and J. M. Delrieu, Magnetism in solid ^{3}He, Rev. Mod. Phys. **55**, 1 (1983).
[44] M. Roger and J. M. Delrieu, Cyclic four-spin exchange on a two-dimensional square lattice: Possible applications in high-tc superconductors, Phys. Rev. B **39**, 2299 (1989).
[45] M. Roger, Ring exchange and correlated fermions, J. Phys. Chem. Solids **66**, 1412 (2005).
[46] H. Weimer, M. Muller, I. Lesanovsky, P. Zoller, and H. P. Büchler, A Rydberg quantum simulator, Nat. Phys. **6**, 382 (2010).
[47] A. W. Glaetzle, M. Dalmonte, R. Nath, I. Rousochatzakis, R. Moessner, and P. Zoller, Quantum Spin-Ice and Dimer Models with Rydberg Atoms, Phys. Rev. X **4**, 041037 (2014).
[48] F. M. Surace, P. P. Mazza, G. Giudici, A. Lerose, A. Gambassi, and M. Dalmonte, Lattice gauge theories and string dynamics in Rydberg atom quantum simulators, arXiv:1902.09551.
[49] D. Barredo, S. de Leseleuc, V. Lienhard, T. Lahaye, and A. Browaeys, An atom-by-atom assembler of defect-free

arbitrary two-dimensional atomic arrays, Science **354**, 1021 (2016).
[50] M. Endres, H. Bernien, A. Keesling, H. Levine, E. R. Anschuetz, A. Krajenbrink, C. Senko, V. Vuletic, M. Greiner, and M. D. Lukin, Atom-by-atom assembly of defect-free one-dimensional cold atom arrays, Science **354**, 1024 (2016).
[51] H. Kim, W. Lee, H.-G. Lee, H. Jo, Y. Song, and J. Ahn, In situ single-atom array synthesis using dynamic holographic optical tweezers, Nat. Commun. **7**, 13317 (2016).
[52] C. Robens, J. Zopes, W. Alt, S. Brakhane, D. Meschede, and A. Alberti, Low-Entropy States of Neutral Atoms in Polarization-Synthesized Optical Lattices, Phys. Rev. Lett. **118**, 065302 (2017).
[53] D. O. de Mello, D. Schäffner, J. Werkmann, T. Preuschoff, L. Kohfahl, M. Schlosser, and G. Birkl, Defect-Free Assembly of 2D Clusters of More Than 100 Single-Atom Quantum Systems, Phys. Rev. Lett. **122**, 203601 (2019).
[54] V. J. Emery, Theory of High-t_c Superconductivity in Oxides, Phys. Rev. Lett. **58**, 2794 (1987).
[55] A. Auerbach, *Interacting Electrons and Quantum Magnetism* (Springer, Berlin, 1998).
[56] A. M. Toader, J. P. Goff, M. Roger, N. Shannon, J. R. Stewart, and M. Enderle, Spin Correlations in the Paramagnetic Phase and Ring Exchange in La_2CuO_4, Phys. Rev. Lett. **94**, 197202 (2005).
[57] B. Paredes and I. Bloch, Minimum instances of topological matter in an optical plaquette, Phys. Rev. A **77**, 023603 (2008).
[58] H.-N. Dai, B. Yang, A. Reingruber, H. Sun, X.-F. Xu, Y.-A. Chen, Z.-S. Yuan, and J.-W. Pan, Four-body ring-exchange interactions and anyonic statistics within a minimal toric-code Hamiltonian, Nat. Phys. **13**, 1195 (2017).
[59] F. D. M. Haldane, Continuum dynamics of the 1-d Heisenberg anti-ferromagnet—identification with the O(3) non-linear sigma-model, Phys. Lett. **93A**, 464 (1983).
[60] T. Kennedy, Exact diagonalisations of open spin-1 chains, J. Phys. Condens. Matter **2**, 5737 (1990).
[61] T. Kennedy and H. Tasaki, Hidden symmetry breaking and the Haldane phase in $s = 1$ quantum spin chains, Commun. Math. Phys. **147**, 431 (1992).
[62] See Supplemental Material at http://link.aps.org/supplemental/10.1103/PhysRevLett.124.073601 for more details of our calculations and extensions to more general settings, which includes Refs. [63,64].
[63] I. Affleck, T. Kennedy, E. H. Lieb, and H. Tasaki, Rigorous Results on Valence-Bond Ground States in Antiferromagnets, Phys. Rev. Lett. **59**, 799 (1987).
[64] F. Pollmann, E. Berg, A. M. Turner, and M. Oshikawa, Symmetry protection of topological phases in one-dimensional quantum spin systems, Phys. Rev. B **85**, 075125 (2012).
[65] M. Murphy, L. Jiang, N. Khaneja, and T. Calarco, High-fidelity fast quantum transport with imperfect controls, Phys. Rev. A **79**, 020301(R) (2009).
[66] M. Müller, I. Lesanovsky, H. Weimer, H. P. Büchler, and P. Zoller, Mesoscopic Rydberg Gate Based on Electromagnetically Induced Transparency, Phys. Rev. Lett. **102**, 170502 (2009).
[67] M. Fleischhauer, A. Imamoglu, and J. P. Marangos, Electromagnetically induced transparency: Optics in coherent media, Rev. Mod. Phys. **77**, 633 (2005).
[68] F. D. M. Haldane, Non-Linear Field-Theory of Large-Spin Heisenberg Anti-Ferromagnets—Semi-Classically Quantized Solitons of the One-Dimensional Easy-Axis Neel State, Phys. Rev. Lett. **50**, 1153 (1983).
[69] A. Läuchli, G. Schmid, and M. Troyer, Phase diagram of a spin ladder with cyclic four-spin exchange, Phys. Rev. B **67**, 100409 (2003).
[70] C. Weitenberg, M. Endres, J. F. Sherson, M. Cheneau, P. Schauss, T. Fukuhara, I. Bloch, and S. Kuhr, Single-spin addressing in an atomic Mott insulator, Nature (London) **471**, 319 (2011).
[71] A. Metavitsiadis and S. Eggert, Competing phases in spin ladders with ring exchange and frustration, Phys. Rev. B **95**, 144415 (2017).